

## Reaction behavior and wear properties of in-situ air plasma-sprayed $\text{Al}_2\text{O}_3\text{-TiB}_2$ composite coatings

Mirhosseini, Seyed Hossein; Mosallae, Masoud; Razavi, Mansour; Fotouhi, Mohammad

**DOI**

[10.1016/j.jeurceramsoc.2023.06.067](https://doi.org/10.1016/j.jeurceramsoc.2023.06.067)

**Publication date**

2023

**Document Version**

Final published version

**Published in**

Journal of the European Ceramic Society

**Citation (APA)**

Mirhosseini, S. H., Mosallae, M., Razavi, M., & Fotouhi, M. (2023). Reaction behavior and wear properties of in-situ air plasma-sprayed  $\text{Al}_2\text{O}_3\text{-TiB}_2$  composite coatings. *Journal of the European Ceramic Society*, 43(14), 6482-6492. <https://doi.org/10.1016/j.jeurceramsoc.2023.06.067>

**Important note**

To cite this publication, please use the final published version (if applicable). Please check the document version above.

**Copyright**

Other than for strictly personal use, it is not permitted to download, forward or distribute the text or part of it, without the consent of the author(s) and/or copyright holder(s), unless the work is under an open content license such as Creative Commons.

**Takedown policy**

Please contact us and provide details if you believe this document breaches copyrights. We will remove access to the work immediately and investigate your claim.

***Green Open Access added to TU Delft Institutional Repository***

***'You share, we take care!' - Taverne project***

**<https://www.openaccess.nl/en/you-share-we-take-care>**

Otherwise as indicated in the copyright section: the publisher is the copyright holder of this work and the author uses the Dutch legislation to make this work public.



# Reaction behavior and wear properties of in-situ air plasma-sprayed $\text{Al}_2\text{O}_3\text{-TiB}_2$ composite coatings

Seyed Hossein Mirhosseini<sup>a</sup>, Masoud Mosallae<sup>a,\*</sup>, Mansour Razavi<sup>b</sup>, Mohammad Fotouhi<sup>c</sup>

<sup>a</sup> Department of Mining and Metallurgical Engineering, Yazd University, Yazd, Iran

<sup>b</sup> Department of Ceramics, Materials and Energy Research Centre, Karaj, Iran

<sup>c</sup> Department of Materials, Mechanics, Management and Design, Delft University of Technology, Delft, the Netherlands

## ARTICLE INFO

### Keywords:

Ceramic Coatings  
In-situ  
Milling  
Plasma spray  
Wear resistance

## ABSTRACT

In this study,  $\text{Al}_2\text{O}_3\text{-TiB}_2$  coating was successfully deposited on steel substrates by in situ plasma spraying (IPS) using  $\text{H}_3\text{BO}_3$ , Al, and  $\text{TiO}_2$  reactants. Beside  $\text{TiB}_2$  and  $\text{Al}_2\text{O}_3$ ,  $\text{Al}_{18}\text{B}_4\text{O}_{33}$  was formed as a by-product with ratio of about 13 wt%. The effect of milling time of reactant and the reaction behavior was also explored. Milling process for at least 10 h can promote efficiency of reaction and milling for efficient production of  $\text{Al}_2\text{O}_3\text{-TiB}_2$  composite. Wear behavior was examined in terms of hardness, wear track width, and wear rate of the coatings with respective measured values of 797.6 HV, 1061.3  $\mu\text{m}$ , and  $4.2 \times 10^{-3} \text{ mm}^3/\text{N.m}$ . Based on the FESEM observations, the thickness of abrasive coating was 417  $\mu\text{m}$ , delamination and adhesion were the main wear mechanisms in  $\text{Al}_2\text{O}_3\text{-TiB}_2$ -coated specimens.

## 1. Introduction

Diverse coating processes have been discussed in the literature. Chemical vapor deposition (CVD) is a low-efficiency method for the deposition of mostly thin films (not coatings) with thicknesses less than 100  $\mu\text{m}$ . Laser cladding is another method for applying coatings, but this method fails in providing uniform and controlled thickness. Another coating method is vacuum plasma spraying which is not cost-effective. Atmospheric plasma sprayed coatings can offer several advantages such as high efficiency, high final thickness, high temperature, and user-friendly operation. However, this method can result in high number of pores and cracks due to poor sinterability of ceramic powders due to low plasma contact time and high melting point of the powders. In-situ plasma spray is a reliable method which combines the benefits of SHS process with APS. IPS method provides more heat through the exothermic combustion reactions which can promote melting of powders, preventing residual unmelted particles, resulting in better densification and decreasing defects. Submicron and nanoscale microstructure can be obtained through this method. Better reinforcing agent-matrix bonding, low production cost, thermodynamically stable final products and acceptable high temperature application are among the other features of the IPS method [1–3].

IPS also enables the formation of coatings through the reaction

between the introduced raw materials and the reactive gases in the plasma. For example, TiN IPS coating is manufactured by reaction between titanium powder and nitrogen carrier gas. Compositions like TiN, AlN, etc are also produced with the aid of Ar/ $\text{N}_2$  plasma gas. Thus, this method relies on the formation of thermodynamically favorable phases through the reaction between raw materials. In other compositions like  $\text{Al}_2\text{O}_3\text{-TiB}_2$ , the raw materials and plasma gas do not react with each other and plasma gas provides necessary energy for combustion reaction between raw materials [4].

Alumina is characterized by its high melting point, high hardness, thermal stability, and corrosion resistance [5]. However, the use of alumina as a ceramic material is accompanied by some limitations due to its low fracture toughness, poor strength, minor impact resistance, and poor thermal shock resistance. As one of the most important engineering ceramic oxides, alumina failed to offer sufficient strength, impact resistance, toughness, and hardness in many applications. Therefore, huge efforts have been made to resolve these issues by compositing and dispersing hard fine particles such as borides [6–8]. Moreover, alumina has been recently combined with a second component to improve its properties.

Among the ultra-high temperature ceramics,  $\text{TiB}_2$  is of great interest due to its high electrical conductivity, chemical stability against molten non-ferrous metals, high melting point (3225°C), and good mechanical

\* Corresponding author.

E-mail address: [mosal@yazd.ac.ir](mailto:mosal@yazd.ac.ir) (M. Mosallae).

<https://doi.org/10.1016/j.jeurceramsoc.2023.06.067>

Received 13 November 2022; Received in revised form 20 June 2023; Accepted 27 June 2023

Available online 28 June 2023

0955-2219/© 2023 Elsevier Ltd. All rights reserved.

**Table 1**  
Characterization of the starting materials.

Materials	Company	Average particle size ( $\mu\text{m}$ )
TiO <sub>2</sub>	SDfine Art: 40446	< 44
H <sub>3</sub> BO <sub>3</sub>	Merck- 100165	< 100
Al	Avl metal- FLPN25	< 25

properties such as strength, hardness, and wear resistance along with relatively low specific weight [9].

Al<sub>2</sub>O<sub>3</sub>-TiB<sub>2</sub> in-situ composites are used both in the bulk and coating forms in the advanced structural applications to improve the wear properties of various substrates. Al<sub>2</sub>O<sub>3</sub> coatings prepared by PVD and

CVD methods have been studied and investigated for engineering applications [10,11]. Several methods such as exothermic dispersion, reactive hot pressing, carbothermal reduction, and aluminothermic reduction have been used to form these composites through the reaction between molten metal and powders such as TiO<sub>2</sub> and B<sub>2</sub>O<sub>3</sub> [12–15]. A limited number of studies have reported the simultaneous formation of these coatings. However, Tekmen et al. [4] produced the Al<sub>2</sub>O<sub>3</sub>-TiB<sub>2</sub> coating through in situ reaction, using the plasma spraying method. According to them, spraying conditions affects the intensity of the reaction. Moreover the resulting coating showed high hardness, making it a suitable option for wear-resistant coatings. Also Lili et al. [16] produced TiB<sub>2</sub>- Al<sub>2</sub>O<sub>3</sub> composite coatings on steel HT200 by in-situ melting

**Table 2**  
Parameters of the APS coating process.

Gun Type	Argon flow rate (SCFH)	Hydrogen gas flow rate (SCFH)	Current (A)	Voltage (V)	Powder feed rate (Lbs./Hr.)	Spray distance (Cm)
3MB Metco	80	15	500	55	25	8

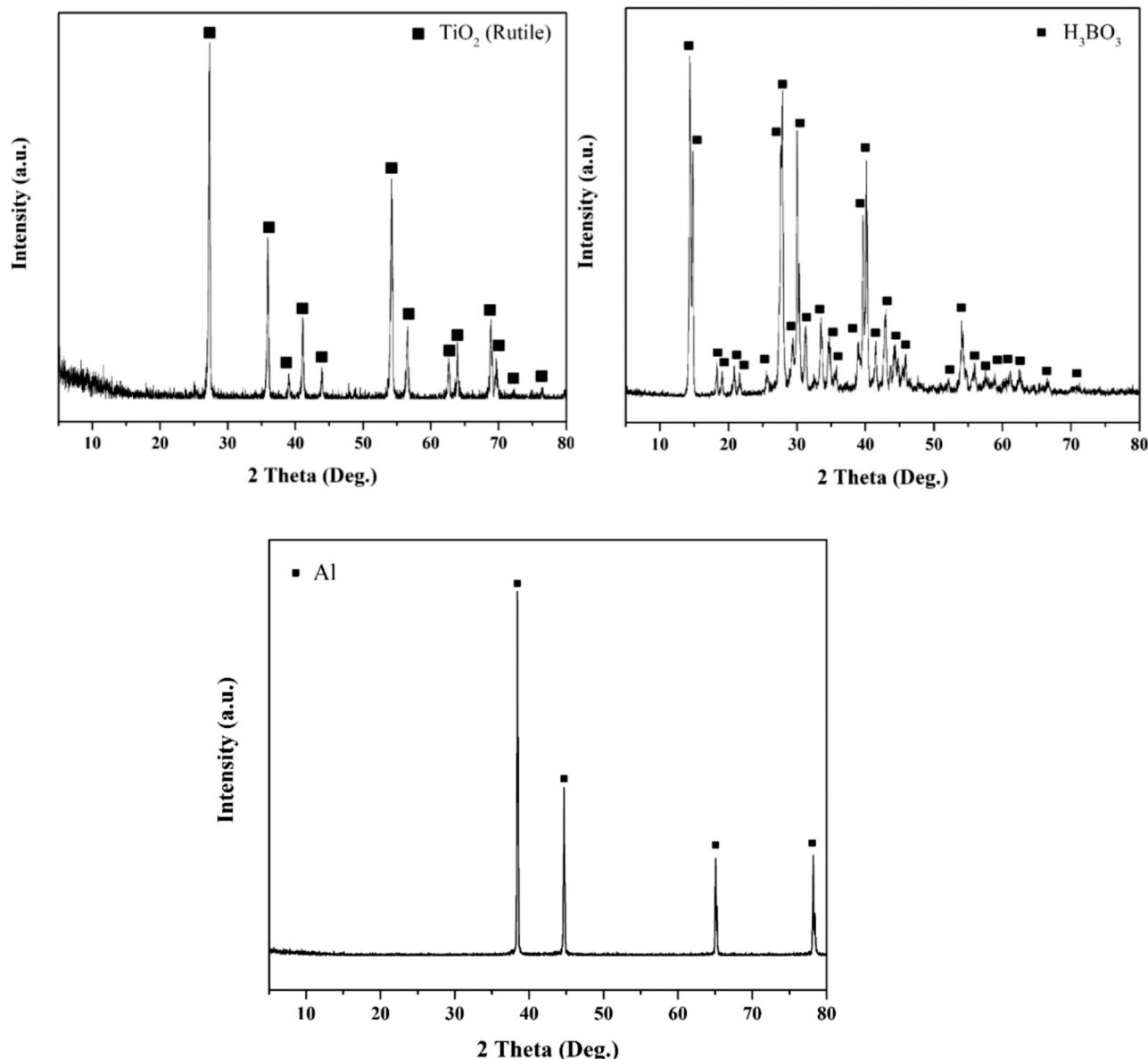


Fig. 1. XRD patterns of raw materials.

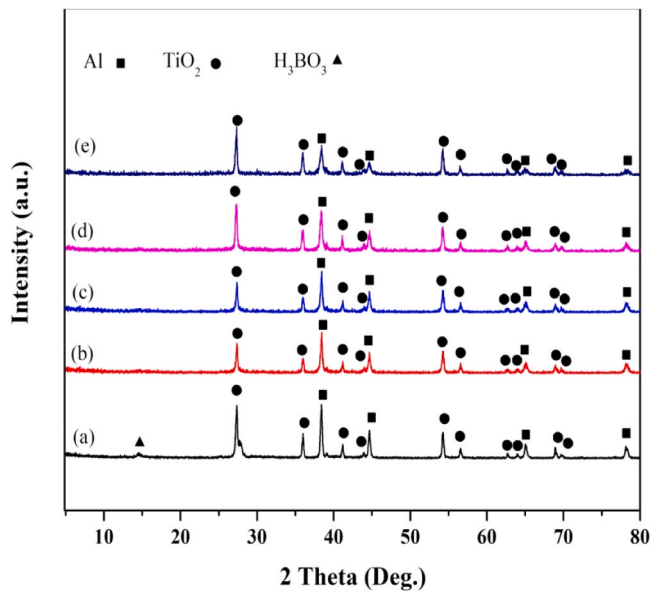


Fig. 2. XRD pattern of raw materials after milling for a) 0, b) 1.5, c) 3, d) 6, and e) 10 h.

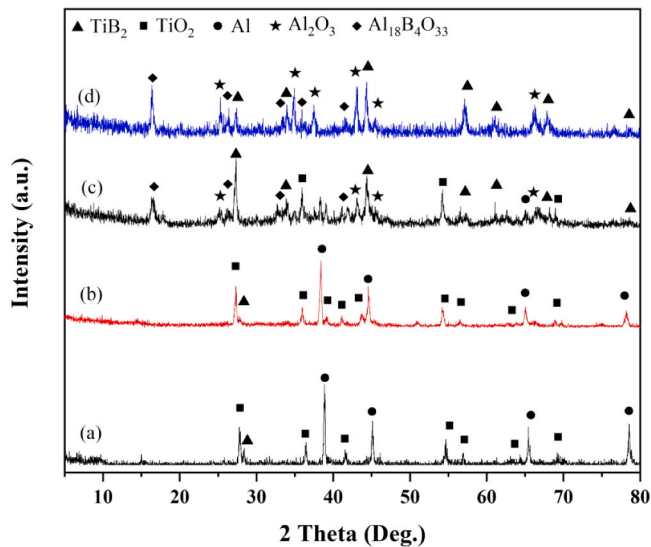


Fig. 3. XRD pattern of samples after coating by APS: a) 1.5(AT1), b) 3(AT3), c) 6(AT6) and d) 10 h(AT10) milling.

reaction and reported two regions; 1)  $\text{TiB}_2$  aggregates and intermixed area of  $\text{TiB}_2$  and  $\text{Al}_2\text{O}_3$  with respective microhardness values of about 2400–3800 HV and 1800–3200HV. Cheng et al. [17] deposited  $\text{Al}_2\text{O}_3$ -30 wt%  $\text{TiB}_2$  composite powder (commercially available) on medium carbon steel substrate with proper wear resistance.

**Table 3**  
Quantitative evaluation of composite coatings calculated by Rietveld refinement technique.

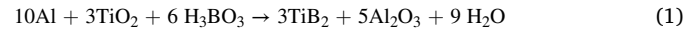
Sample	Identified phases	Weight fraction (%)		Crystal system	Space group
		Before PS	After PS		
AT10	Al	30.64	0	cubic	Fm-3 m
	$\text{H}_3\text{BO}_3$	42.14	0	-	-
	$\text{TiO}_2$	27.22	0	tetragonal	P42/m n m
	$\text{Al}_2\text{O}_3$	0	57.77	trigonal	R-3c:H
	$\text{TiB}_2$	0	28.69	hexagonal	P6/m m m
	$\text{Al}_{18}\text{B}_4\text{O}_{33}$	0	13.53	orthorhombic	CmC21

In this article, the reactions behavior and the effect of milling time of  $\text{H}_3\text{BO}_3 + \text{TiO}_2 + \text{Al}$  mixtures on the formation of in-situ  $\text{TiB}_2\text{-Al}_2\text{O}_3$  coatings are investigated during the air plasma spraying process. Moreover, the properties of the prepared coatings such as their hardness and wear behavior are evaluated.

## 2. Experimental procedure

### 2.1. Preparation of raw materials and coatings

Table 1 lists the specifications of the raw materials used in this study. Definite weights of powders according to the stoichiometric ratios of reaction 1 [18] were milled using a planetary ball mill.



$$\Delta H_{(298)} = -2518.9(\text{KJ/mol})$$

Both balls and milling medium were made of stainless steel. The mixture of titanium oxide ( $\text{TiO}_2$ ), boric acid ( $\text{H}_3\text{BO}_3$ ), and aluminum (Al) powders were milled for 0–10 h at a speed of 250 rpm with a ball-to-powder ratio of 15:1. The mixed powder (0 h) and powder milled for 1.5, 3, 6 and 10 h (which are respectively labeled as AT1, AT3, AT6, and AT10) were used in the coating preparation. These four batches were granulated to prepare coatings by atmospheric plasma spray (APS) method.

The size of granules ranged between 45 and 75  $\mu\text{m}$ . Before spraying, the substrate was sand blasted and cleaned by acetone to enhance the adherence between the ceramic coating and metallic substrate. Details of the processing parameters can be found in Table 2 which were optimized in a previous work [19].

### 2.2. Characterization of the Coatings

After plasma spraying, microhardness of the samples was measured using Vickers indentation method with the load of 200 g and holding time of 15 s. At least 5 indentations were performed for each sample and the average result was reported. The wear behavior was investigated by pin-on-disk method with a tungsten carbide (WC) pin (diameter = 5 mm, hardness = 75 HRC) as a counterbody [20]. The sliding speed and distance were set 0.07 m/s and 200 m, respectively; while the applied normal load was 3 N. The WC pin was located 10 mm (internal diameter: 20 mm) apart from the center of samples.

The sensors in the pin-on-disk apparatus documented the coefficient of friction during the experiment. The wear rate was calculated following the verification of the worn area width based on this procedure:  $\text{Wear rate} = V / (N.S)$ , In which, V is the volume loss of the specimen ( $\text{mm}^3$ ), N denotes the applied load (N), and S represents the sliding distance (m). The volume loss was determined based on the following equation:

$$\text{Volume loss (V)} = (\pi R d^3) / 6r \quad (2)$$

Where R is the wear track radius (mm), d refers to the wear track width (mm), and r is the pin radius (mm) after the wear tests [21].

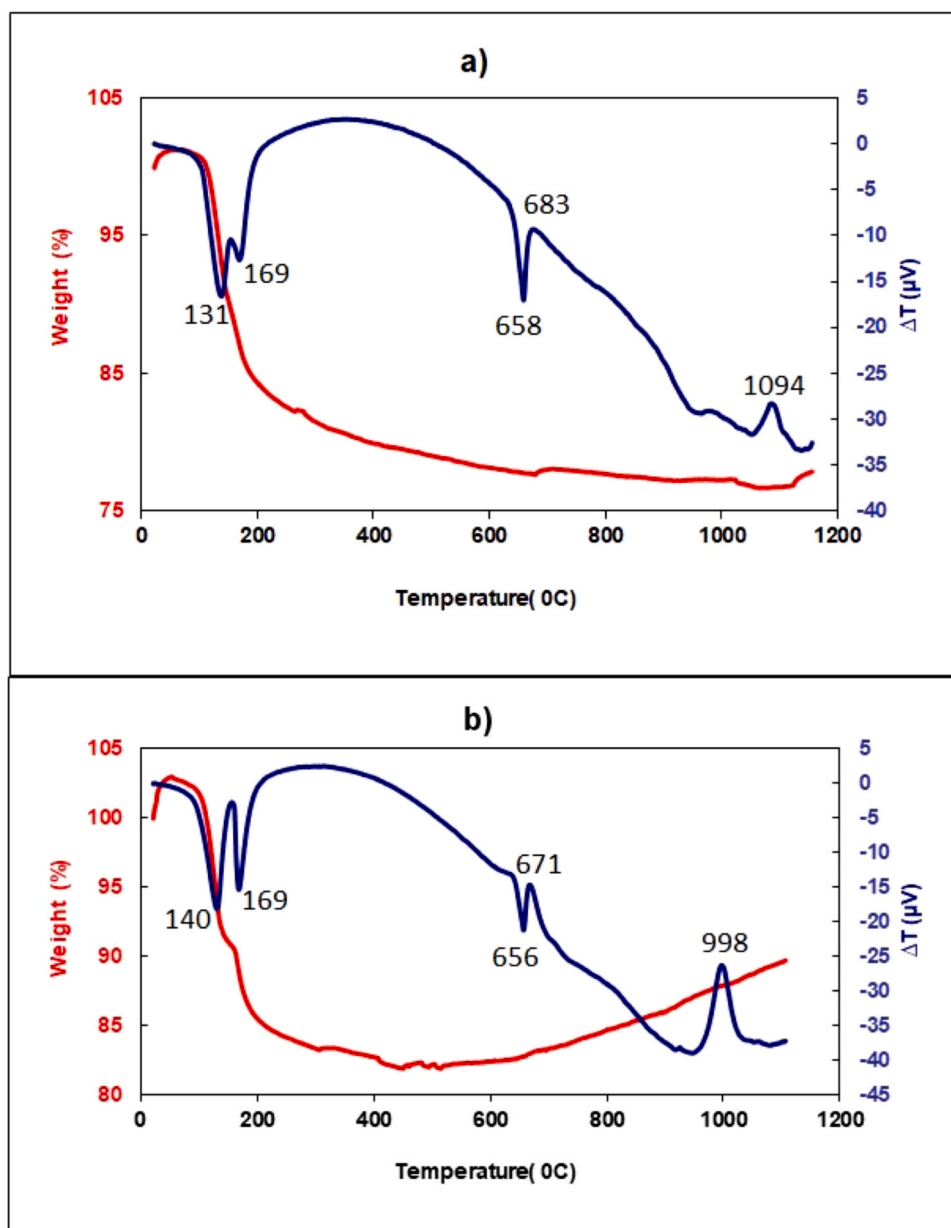


Fig. 4. DTA analysis of a) unmilled and b) milled raw materials.

### 2.3. Characterization methods

The phase of the coatings was identified by X-ray diffraction (XRD) method using a Siemens D-500 X-ray diffractometer equipped with  $\text{CuK}\alpha$  radiation ( $\lambda = 1.54 \text{ \AA}$  at 20 kV and 30 mA).

Field emission scanning electron microscopy (TESCAN MIRA3, Czech Republic) was also employed to evaluate the morphology of the coatings. Moreover, the worn surfaces were studied by FESEM equipped with an energy dispersive X-ray (EDX). EDS detector was used to investigate the transfer of elements between samples and WC pin during wear, which can be effective in determining wear mechanisms.

## 3. Results and discussion

### 3.1. Milling of raw materials

XRD patterns of starting materials can be seen in Fig. 1. Milling

process was carried out to boost the contacts between starting particles and activate in situ reaction during plasma spray [4]. It is reported that ball milling for 60 h can lead to the formation of final products through mechanical alloying [22].

Fig. 2 shows XRD pattern of raw materials after milling. As seen, there is no change in the composition of starting material even after milling for 10 h and the expected products i.e.  $\text{Al}_2\text{O}_3$  and  $\text{TiB}_2$  did not form. After milling,  $\text{H}_3\text{BO}_3$  peaks disappeared probably due to three reasons: the amount of  $\text{H}_3\text{BO}_3$  is lower than Al according to stoichiometric ratios of reaction 1. Secondly, the intensity of  $\text{H}_3\text{BO}_3$  peak remarkably decremented due to the lower mass absorption coefficient of  $\text{H}_3\text{BO}_3$  (8.92) compared to Al (48.67) and  $\text{TiO}_2$  (121.97). Thirdly, milling process lowered the crystallite size of  $\text{H}_3\text{BO}_3$ .

Fig. 3 shows the XRD pattern of the samples after coating by APS. The required activation energy for the reaction, during the coating process, can be provided by the exposure of the starting powder to high temperature conveying gas during the APS process. No changes were

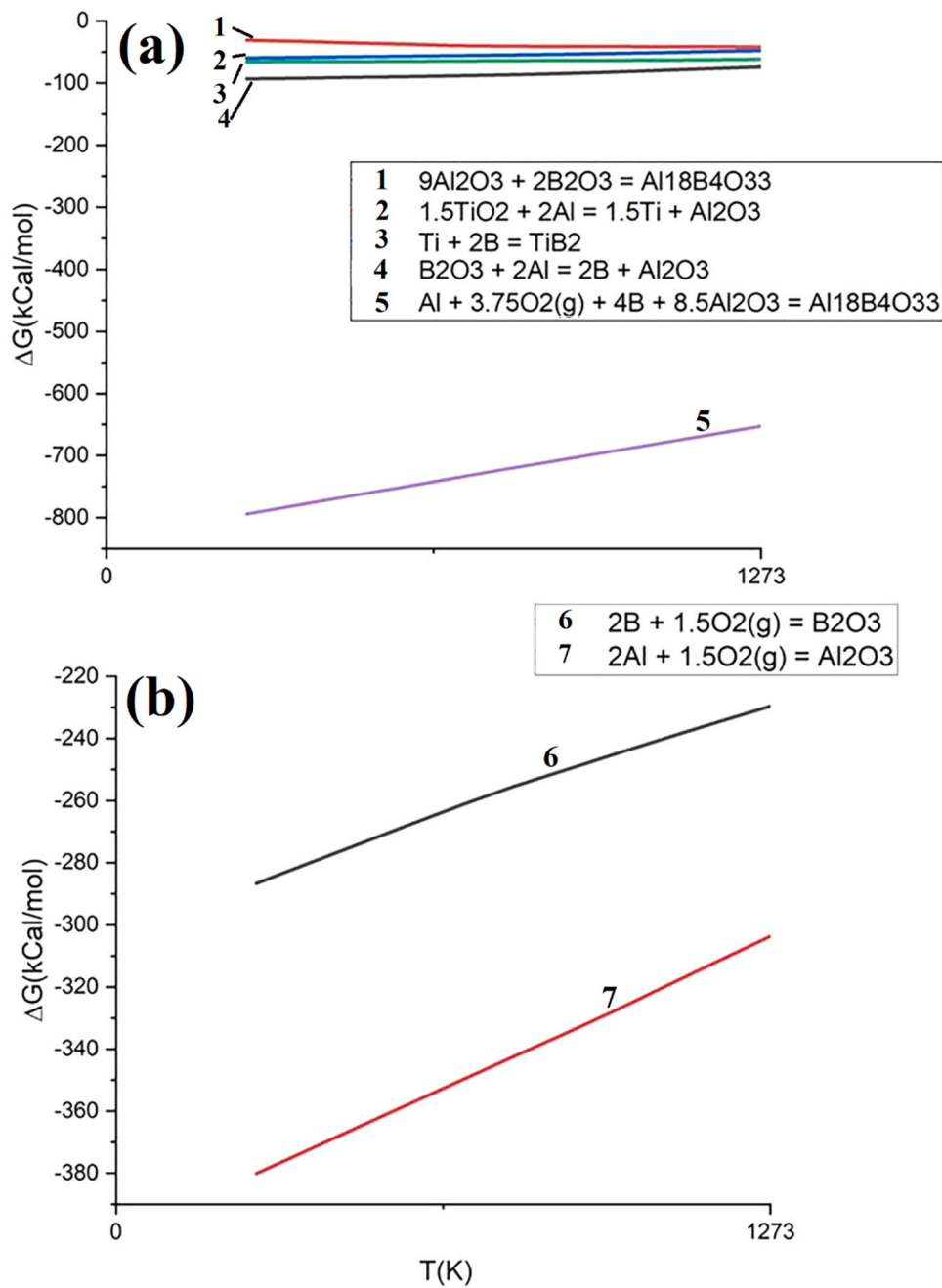


Fig. 5. a) Gibbs Free energies of possible reactions between raw materials vs temperature b) Gibbs Free energies of oxidation of Al and B.

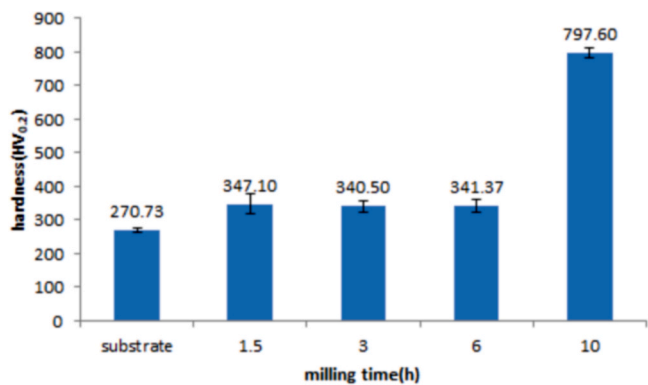


Fig. 6. Hardness of the samples.

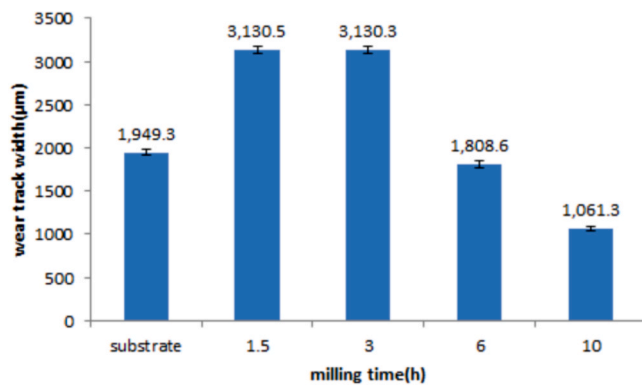


Fig. 7. Wear track width of the substrate and coated samples.

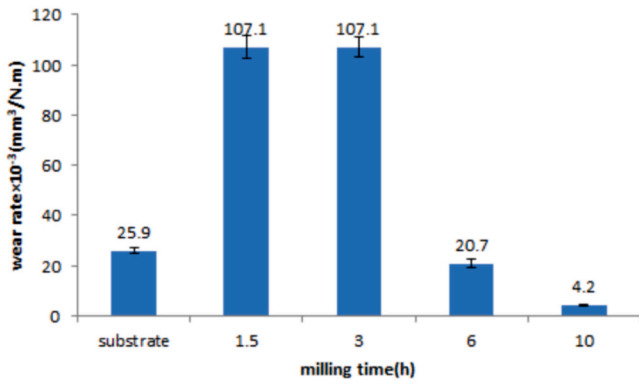


Fig. 8. Wear rate of the substrate and coated samples.

detected in the XRD pattern of AT1 and AT3 after coating (Fig. 3. a and b compared to Fig. 2. b and c), suggesting that the milled raw materials did not react with each other. In the case of AT6 sample, the raw materials (i.

e. Al and TiO<sub>2</sub>) remained after the formation of Al<sub>2</sub>O<sub>3</sub>, TiB<sub>2</sub>, and Al<sub>18</sub>B<sub>4</sub>O<sub>33</sub> phases, (Fig. 3. c). The reaction completed in the AT10 (Fig. 3. d) showing no residual primary phases of Al, TiO<sub>2</sub>, and B<sub>2</sub>O<sub>3</sub>. Based on these results, the necessary ball milling duration for in-situ reaction, significantly decreased from 48 h to 10 h [4]. By-product of the reaction i.e. Al<sub>18</sub>B<sub>4</sub>O<sub>33</sub> is a middle phase, which is a member of borate family with a melting point, density, low linear expansion coefficient, hardness, and elastic modulus of 1440 °C, 2.94 g/cm<sup>3</sup> [23], (4.2 × 10<sup>-6</sup> K<sup>-1</sup>) [24], 12, and 400 GPa, respectively [25].

Crystallographic data of the phases formed by APS coating of the AT10 sample can be examined by Rietveld refinement technique as summarized in Table 3. According to this table, for AT10, all the raw materials were consumed and final composite consisted of 57.77% Al<sub>2</sub>O<sub>3</sub>, 28.69% TiB<sub>2</sub>, and 13.53% Al<sub>18</sub>B<sub>4</sub>O<sub>33</sub> after plasma spray coating.

### 3.2. Investigation of reaction behavior

TG-DTA analysis was performed to examine the effect of milling on reaction behavior of in-situ synthesis of Al<sub>2</sub>O<sub>3</sub>-TiB<sub>2</sub> composite from Al, TiO<sub>2</sub> and H<sub>3</sub>BO<sub>3</sub> powders. Fig. 4. a and b illustrate DTA graphs of

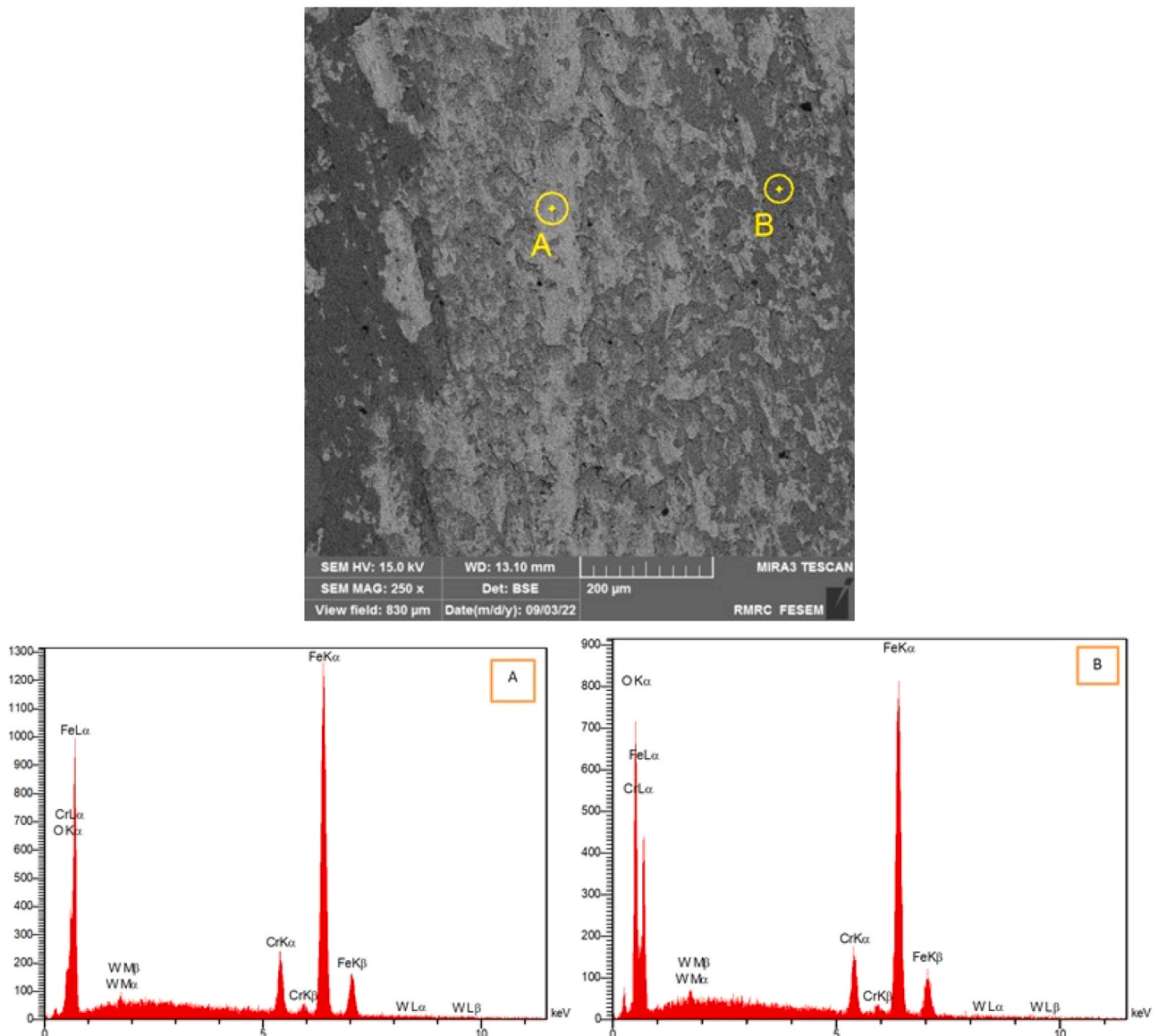


Fig. 9. Wear track of the substrate and EDS analysis.

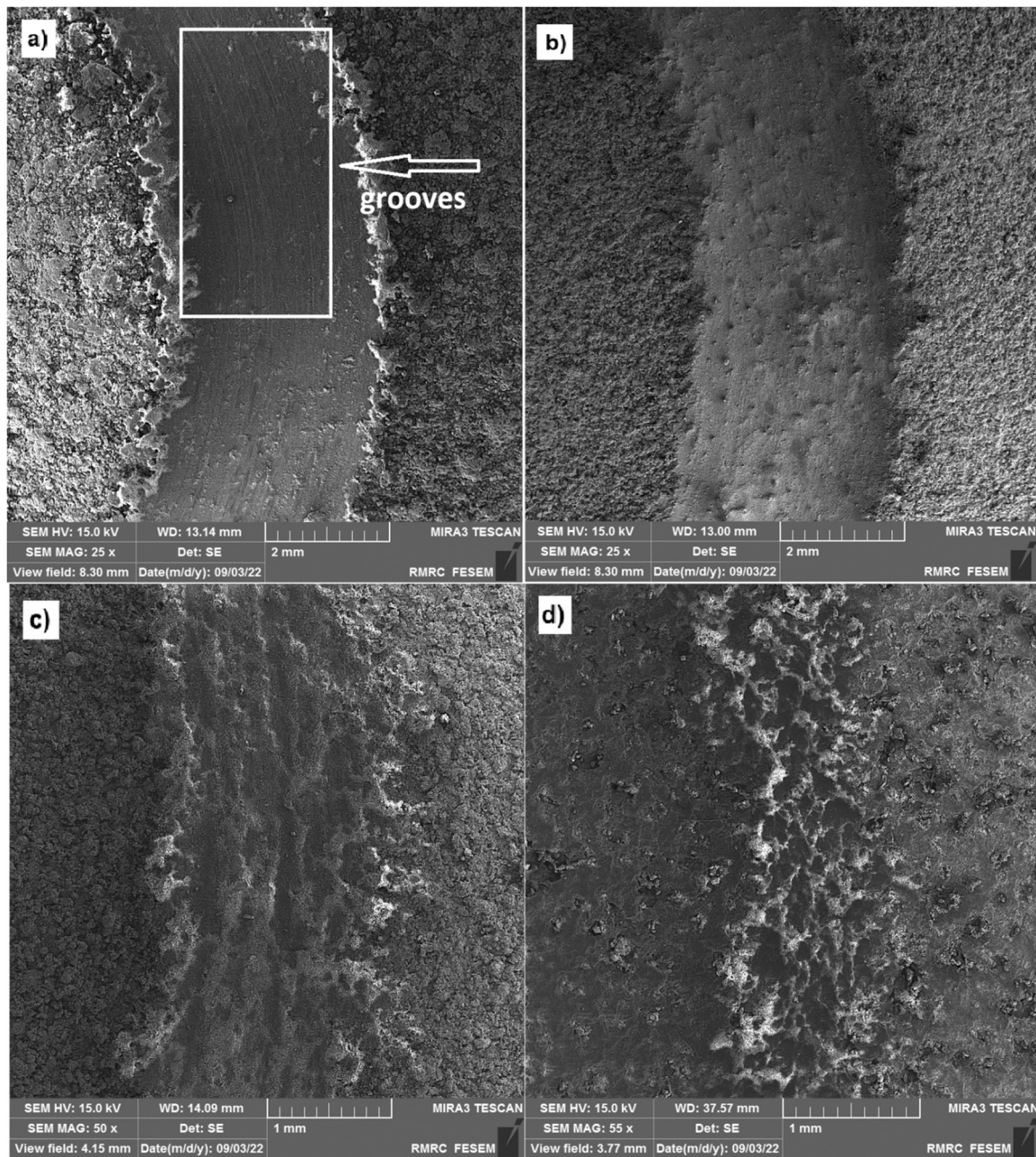
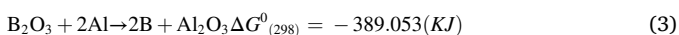
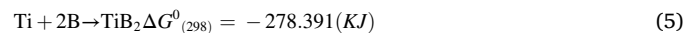
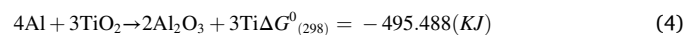


Fig. 10. Wear width track of coated samples: a) AT1, b) AT3, c) AT6, and d) AT10.

unmilled and milled specimens for 10 h. As it can be seen, both graphs show three endothermic peaks. The first one at about 131 (Fig. 4. a) or 140 °C (Fig. 4. b) is related to the removal of absorbed water which led to a severe drop in the TG curve. The next peak emerges at about 169 °C which can be assigned to the decomposition of  $H_3BO_3$  to  $B_2O_3$  and water vapor or disintegration of some unsteady compounds [26,27]. The last endothermic peak at about 658 °C (Fig. 4. A) or 656 °C (Fig. 4. B) can be attributed to melting of Aluminum powder in the specimen. The exothermic peak at 683 °C (in Fig. 4. A) and 671 °C (in Fig. 4. B) can be ascribed to the following reaction [26].



The next exothermic peak of unmilled specimen emerged at about 1094 °C (998 °C for milled sample) due to the formation of  $TiB_2$  through the following two steps [26]:



Based on the results, milling promoted the reactions at lower temperatures and increased the DTA peak intensity, implying more efficiency.

Fig. 5. (a) depicts Gibbs free energy of possible reactions between reactants up to 1273 K. The temperature of the carrier gas exceeds 10,000 °C [28], but regarding the ultra-short contact time between the powder and gas in the IPS process, true temperature cannot be determined, therefore, the thermodynamic data of the reaction are not available. Melting point of  $B_2O_3$  is about 450 °C. Thus, at this temperature, the reactants will be molten  $B_2O_3$  and dispersed Al and  $TiO_2$  particles. It seems that the feasibility of reaction 1 is more than other

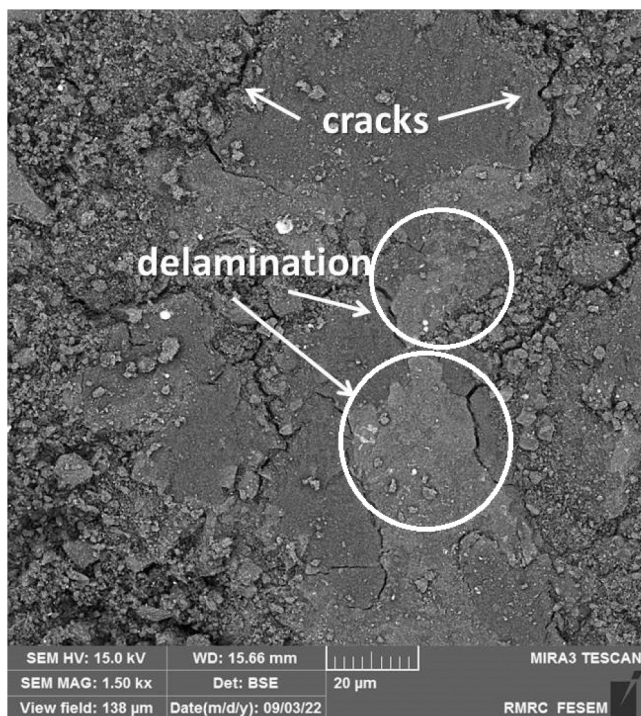


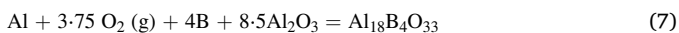
Fig. 11. Worn surface of AT10.

reactions at temperatures below 1273 K and molten  $B_2O_3$  reacts with Al particles, leading to the formation of an alumina shell around Al particles [15]. Then, alumina shell will react with molten  $B_2O_3$  and forms  $Al_{18}B_4O_{33}$  byproduct based on Reaction 5.



On the other hand, plasma spray can result in Al evaporation as reported for Mg in a combustion synthesis process [29]. According to Reaction 1, a part of  $B_2O_3$  will remain unreacted in the Al- $B_2O_3$ - $Al_2O_3$  system which can react with  $Al_2O_3$  product through the above reaction.

Moreover, during plasma spray,  $B_2O_3$  can be extracted from the mixture by vaporization. Consequently, Al cannot be completely consumed by Reaction 1 due to a decline in  $B_2O_3$  content during in the milling process. Therefore,  $Al_2O_3$  product, molten B, Al, and oxygen of atmosphere are present in the reaction medium. Based on Fig. 5. (b), oxidation of Al is more thermodynamically favorable than oxidation of B. Thus,  $Al_{18}B_4O_{33}$  byproduct is formed due to Al oxidization through the following reaction:



When the temperature reaches Al melting point, molten alumina reacts with  $TiO_2$ , leaving free Ti to react with B and form  $TiB_2$ .

### 3.3. Investigation of wear behavior

Hardness measurements of the samples versus the milling time are shown in Fig. 6. Accordingly, the hardness of the coating is associated with in-situ phases, and hence, the milling time. The expected phases did not form completely in AT1 to AT6 specimens, thus, the hardness did not show a significant variation. Maximum coating hardness was achieved in AT10, which was milled for 10 h, giving rise to the complete formation of the  $Al_2O_3$ - $TiB_2$  phases. Compared to previous works, the hardness

of the coating considerably improved from 517 to 797.6 HV<sub>200</sub> [4]. Although higher milling time leads to finer particles and lower porosities, the hardness did not change remarkably from 1.5 h to 6 h milling time. Hardness evaluation test in ceramics often depends on two processes: plastic deformation and microcracking. By decline of the grain size to the nanometer scale, elastic module decreases which enhances the hardness [30]. In the case of micro-scaled grain size, the effect of grain size on the hardness can be neglected [31]. Therefore, the hardness is associated with porosity of the coating. AT1 and AT3 samples are constituted from Al,  $TiO_2$ , and  $H_3BO_3$  which do not have high hardness values. It seems that more milling time did not significantly reduce the porosities. In the AT6,  $Al_2O_3$ ,  $TiB_2$ , and  $Al_{18}B_4O_{33}$  are partially created and presence of raw materials (i.e. Al metallic phase with the hardness of 160–350 MPa [32]) beside  $Al_2O_3$  and  $TiB_2$  led to lower hardness values compared to AT10. Difference between linear expansion coefficients of these phases can lead to microcracking which also lowers the hardness. In the AT10, the complete formation of hard phases of  $Al_2O_3$  and  $TiB_2$  dramatically improved the hardness of the coating.

Fig. 7. shows width of wear track versus the milling time. The wear width of the substrate is 1949.3  $\mu m$ ; while AT1 and AT3 exhibited wear with of 3130  $\mu m$ . Wear width reaches 1808.6  $\mu m$  in AT6 which contains both  $TiB_2$  and  $Al_{18}B_4O_{33}$ . The minimum wear width of 1061.3  $\mu m$  was also observed in the AT10, which agrees with the complete formation of the main phases of  $Al_2O_3$  and  $TiB_2$ . It can be concluded that wear resistance of substrate remarkably improved by in-situ coating. Based on the wear rate calculations (Fig. 8), 10 h of milling led to the best outcomes, where  $Al_2O_3$ - $TiB_2$  composite coating can significantly improve wear resistance of the steel substrate and decrease wear rate by approximately 84%. Wear resistance is not only attributed to hardness, but also associated with the hardness/elastic modulus ratio [33,34]. Longer milling time led to smaller grain size and lower elastic modulus [30]. Despite the similar hardness of AT1, AT3, and AT6, the elastic modulus of the AT6 sample was lower than the others due to its smaller grain size. It can be concluded that H/E ratio and wear resistance of AT6 is higher than AT1 and AT3.

EDS analysis and FESEM observations were also considered to investigate the wear mechanisms. Fig. 9. shows higher magnification of wear track of the substrate with two distinct phases. According to the EDS analysis, the presence of W element on the surface implies the dominance of the adhesive mechanism in the wear process. The presence of oxygen in dark regions is also a sign of the oxidation mechanism.

Wear width track of the AT1, 3, 6 and 10 coatings are shown in Fig. 10. The appearance of the wear track in the AT6 and AT10 samples is different from AT1 and AT3 which can be due to their constitutive phases as discussed earlier. The presence of threads on the wear track of the AT1 specimen suggests the possibility of abrasive mechanism.

Fig. 11. depicts further investigation of the worn surface of AT10 in which the cracks were raised, resulting in the delamination mechanism. As stated in the previous studies, low fracture toughness of ceramic material leads to the growth of the cracks in sub-surfaces of the specimen. The cracks are generated in lower surfaces following the continuous motion of the wear test pin on the coating surface due to the tensions. Cracks grew and finally meet each other, giving rise to the separation of a sheet and delamination [35].

Fig. 12 displays wider wear width track of the AT10 sample at higher magnification. MAP analysis indicates the presence of W on the AT10 surface which is extracted from WC pin, suggesting the existence of the adhesive mechanism [36]. Thanks to its ionic-covalent bonding, the hardness of  $TiB_2$  is more than WC [37]. When the WC pin moves on the  $Al_2O_3$ - $TiB_2$  coating, it faces  $TiB_2$  phase and this interaction can lead to the removal of WC particles. Moreover, detached WC particles on the wear track can serve as an abrasive and take more particles from WC pin;

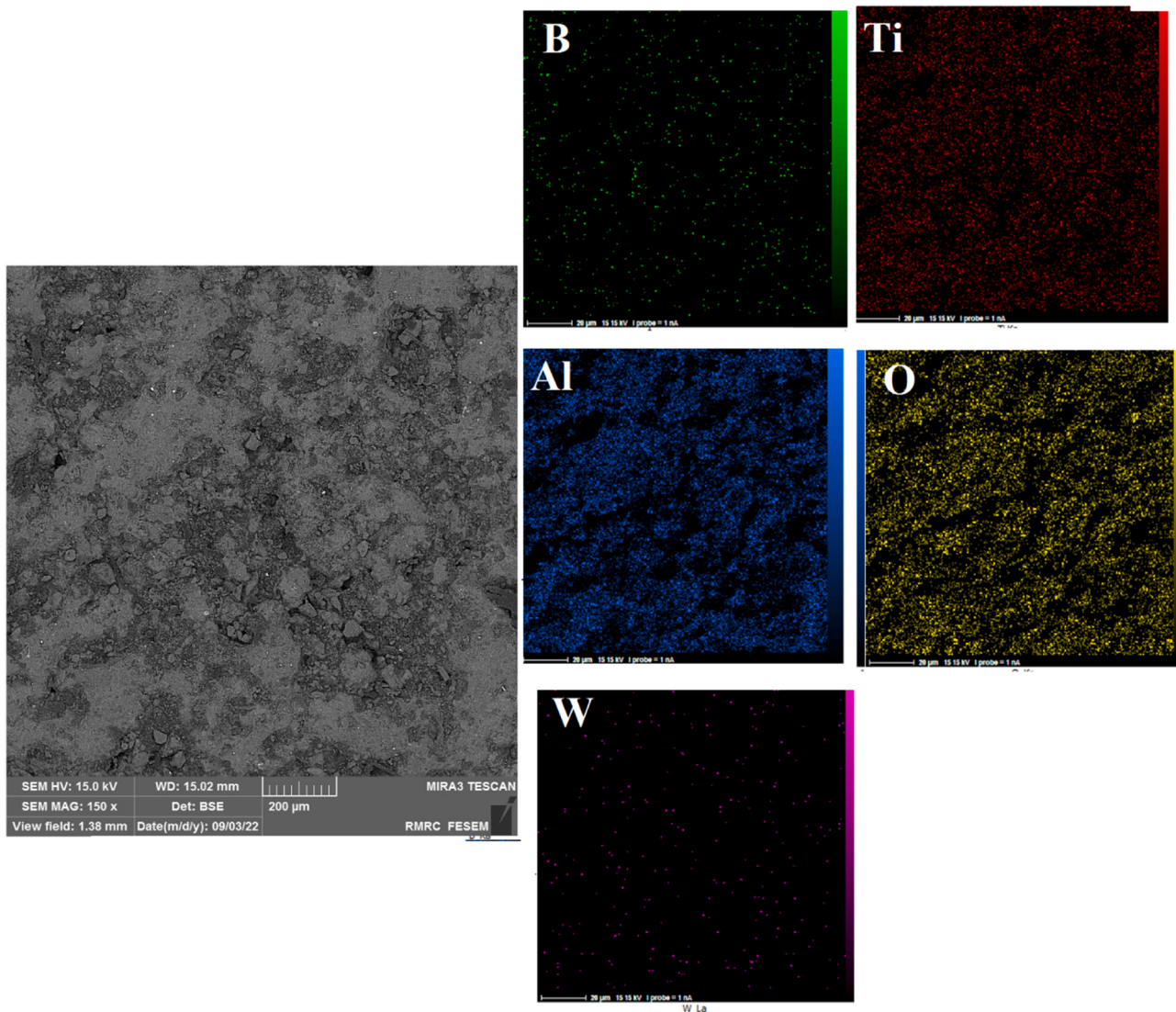


Fig. 12. Map analysis of wear width track of AT10.

finally, the segregated WC particles adhere to the wear surface [35].

Fig. 13. (a) shows AT10 cross-section microscopic image. Fig. 13. (b) depicts the higher magnification of the interface between the coating and steel substrate. No cracks can be found on the surface of the coating due to lack of thermal tension. However, there are some porosities. Based on Fig. 13. (b) there is no gap between the substrate and plasma-sprayed coating, reflecting a their proper adhesion. The coating is homogenous throughout the substrate with the thickness of 417  $\mu\text{m}$ . Fig. 13. (c) shows the microstructure of the AT10 coating in higher magnification. Map analysis reveals existence of Al, O, Ti, B and Fe elements. Fe element probably originates from milling media and balls.

#### 4. Conclusions

In this paper reports the use of the in-situ air plasma spray method to fabricate  $\text{Al}_2\text{O}_3\text{-TiB}_2$  composite coating on steel substrates to achieve a  $\text{H}_3\text{BO}_3\text{-Al-TiO}_2$  system. After the optimization of milling time, reaction behavior and wear behavior of the coated samples were studied. The main results of this research can be summarized as follows:

1. The final  $\text{Al}_2\text{O}_3\text{-TiB}_2$  composite coating consisted of 57.77%  $\text{Al}_2\text{O}_3$ , 28.69%  $\text{TiB}_2$ , and 13.53%  $\text{Al}_{18}\text{B}_4\text{O}_{33}$ . By this procedure, all of the reactants were consumed and participated in the reaction.
2. Study of  $\text{Al}_{18}\text{B}_4\text{O}_{33}$  by-product showed that this phase can be originated from three main routes: the formation of Al-alumina core-shell structure, reduction of Al or  $\text{B}_2\text{O}_3$  reactants by vaporization during IPS.
3. The milling process promoted the reactions at lower temperatures. Furthermore, milling time was optimized. At least 10 h of milling is needed to form complete composite after IPS. Compared to previous studies, this method considerably reduced the milling time from 48 h to 10 h.
4. Compared to previous works, the homogeneous 417  $\mu\text{m}$  thick  $\text{Al}_2\text{O}_3\text{-TiB}_2$  coating showed favorable mechanical properties including hardness of 797.6 HV, wear track width of 1061.3  $\mu\text{m}$ , and wear rate of  $4.2 \times 10^{-3} \text{ mm}^3/\text{N.m}$ .  $\text{Al}_2\text{O}_3\text{-TiB}_2$  composite coating can significantly decrease wear rate of steel substrate by approximately 84%.
5. Based on FESEM observations, abrasion, delamination, and adhesion are the major active wear mechanisms, governing the wear performance of the  $\text{Al}_2\text{O}_3\text{-TiB}_2$ -coated specimens.

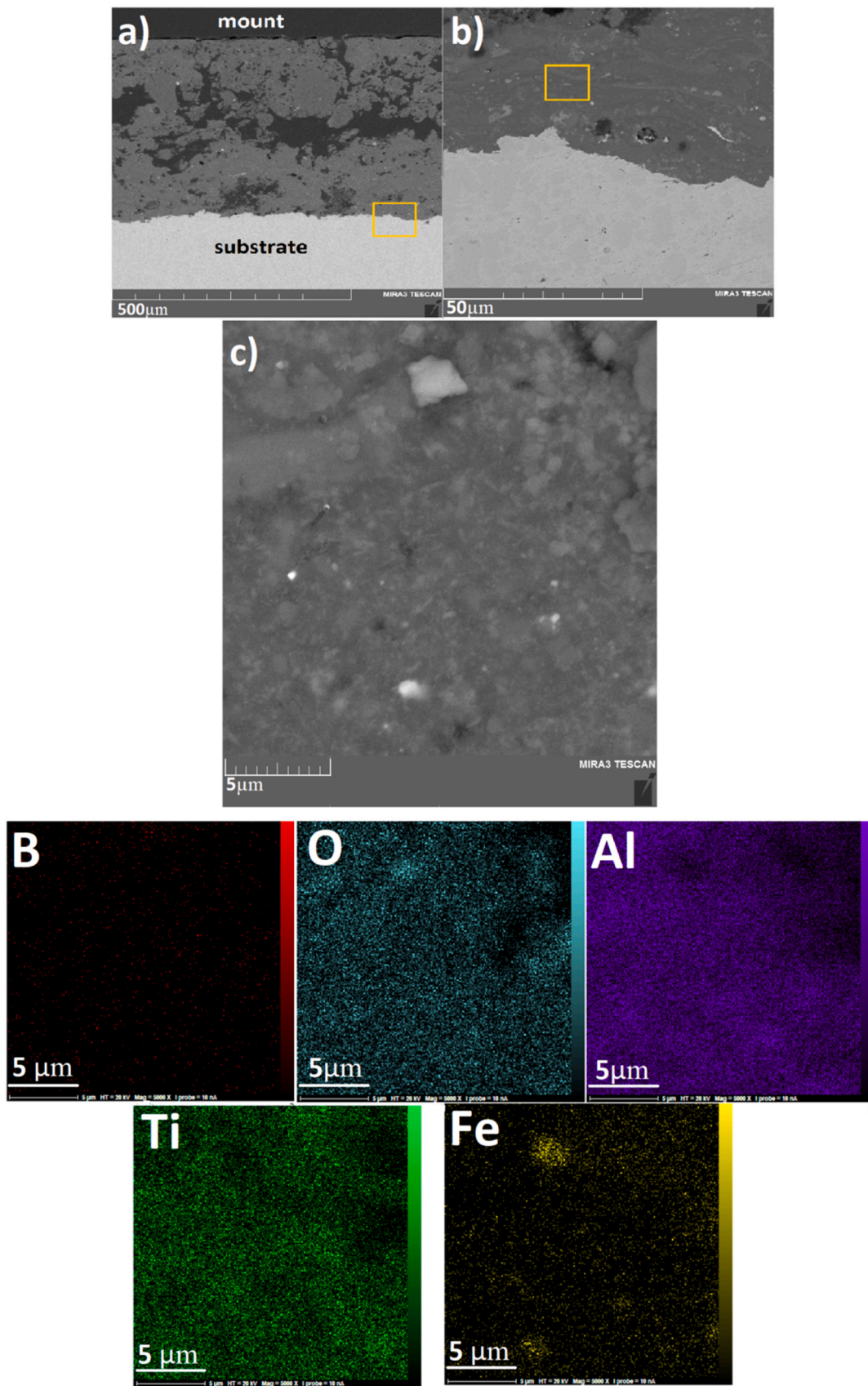


Fig. 13. (a). AT10 cross section, (b). Higher magnification of coating-substrate interface (c) Higher magnification of coating microstructure and its map analysis.

## Declaration of Competing Interest

The authors declare that they have no known competing financial interests or personal relationships that could have appeared to influence the work reported in this paper.

## References

- [1] Y.X. Shao, Y. Yang, L. Wang, C.C. Zhao, Y.W. Wang, Y.D. Ma, Y.H. Cui, W.W. Sun, X.Y. Wang, L. Wang, Y. Wang, Microstructure characterization of in-situ ZrC composite coating with graceful toughness and improved tribological properties prepared by plasma spraying, *Mater. Charact.* vol. 179 (2021), 111382.
- [2] X. Wang, Y. Yang, S. Jia, Y. Wang, Y. Ma, Y. Cui, X. Wang, W. Sun, L. Wang, In-situ synthesis, microstructure, and properties of NbB<sub>2</sub>-NbC-Al<sub>2</sub>O<sub>3</sub> composite coatings by plasma spraying, *J. Adv. Ceram.* vol. 11 (8) (2022) 1263–1278.
- [3] H. Mindivan, C. Tekmen, B. Dikici, Y. Tsunekawa, M. Gavali, Wear behavior of plasma sprayed composite coatings with in situ formed Al<sub>2</sub>O<sub>3</sub>, *Mater. Des.* vol. 30 (10) (2009) 4516–4520.
- [4] C. Tekmen, Y. Tsunekawa, M. Okumiya, In-situ TiB<sub>2</sub> and Al<sub>2</sub>O<sub>3</sub> formation by DC plasma spraying, *Surf. Coat. Technol.* vol. 202 (17) (2008) 4170–4175.
- [5] A.M. Abyzov, Aluminum oxide and alumina ceramics (review). Part 1. Properties of Al<sub>2</sub>O<sub>3</sub> and commercial production of dispersed Al<sub>2</sub>O<sub>3</sub>, *Refract. Ind. Ceram.* vol. 60 (1) (2019) 24–32.
- [6] I. Kimura, N. Hotta, Y. Hiraoka, N. Saito, Y. Yokota, Sintering and characterization of Al<sub>2</sub>O<sub>3</sub>-TiB<sub>2</sub> composites, *J. Eur. Ceram. Soc.* vol. 5 (1) (1989) 23–27.
- [7] J. Xu, B. Zou, S. Tao, M. Zhang, X. Cao, Fabrication and properties of Al<sub>2</sub>O<sub>3</sub>-TiB<sub>2</sub>-TiC/Al metal matrix composite coatings by atmospheric plasma spraying of SHS powders, *J. Alloy. Compd.* vol. 672 (2016) 251–259.
- [8] D. Jianxin, Friction and wear behaviour of Al<sub>2</sub>O<sub>3</sub>/TiB<sub>2</sub>/SiCw ceramic composites at temperatures up to 800C, *Ceram. Int.* vol. 27 (2) (2001) 135–141.
- [9] B.R. Golla, T. Bhandari, A. Mukhopadhyay, B. Basu, Titanium diboride, *Ultra Temp. Ceram. Mater. Extrem. Environ. Appl.* (2014) 316–360.
- [10] M. Åstrand, T.I. Selinder, F. Fietzke, H. Klostermann, PVD-Al<sub>2</sub>O<sub>3</sub>-coated cemented carbide cutting tools, *Surf. Coat. Technol.* vol. 188 (2004) 186–192.
- [11] S. Ruppi, Deposition, microstructure and properties of texture-controlled CVD α-Al<sub>2</sub>O<sub>3</sub> coatings, *Int. J. Refract. Met. Hard Mater.* vol. 23 (4–6) (2005) 306–316.
- [12] H.-G. Zhu, H.-Z. Wang, L.-Q. Ge, C. Shi, S.-Q. Wu, Formation of composites fabricated by exothermic dispersion reaction in Al-TiO<sub>2</sub>-B<sub>2</sub>O<sub>3</sub> system, *Trans. Nonferrous Met. Soc. China* vol. 17 (3) (2007) 590–594.
- [13] H. Huang, In situ reactive hot press sintering and mechanical properties of Al<sub>2</sub>O<sub>3</sub>-TiB<sub>2</sub>-B<sub>4</sub>C composites, *J. Mater. Sci.* vol. 51 (7) (2016) 3481–3489.
- [14] D. Wang, Effects of additives on combustion synthesis of Al<sub>2</sub>O<sub>3</sub>-TiB<sub>2</sub> ceramic composite, *J. Eur. Ceram. Soc.* vol. 29 (8) (2009) 1485–1492.
- [15] V. Sundaram, K.V. Logan, R.F. Speyer, Aluminothermic reaction path in the synthesis of a TiB<sub>2</sub>-Al<sub>2</sub>O<sub>3</sub> composite, *J. Mater. Res.* vol. 12 (7) (1997) 1681–1684.
- [16] C. Lili, C. Hongzhi, and C. Yunbo, Preparation and microstructure of TiB<sub>2</sub>/Al<sub>2</sub>O<sub>3</sub> composite coating by melting in-situ reaction processing, 2010.
- [17] H.C. Cheng, Z.X. Li, Y.W. Shi, Microstructure and wear resistance of Al<sub>2</sub>O<sub>3</sub>-TiB<sub>2</sub> composite coating deposited by axial plasma spraying, *Surf. Eng.* vol. 24 (6) (2008) 452–457.
- [18] R.T. Mousavian, S. Sharafi, M.R. Roshan, M.H. Shariat, Effect of mechanical activation of reagents' mixture on the high-temperature synthesis of Al<sub>2</sub>O<sub>3</sub>-TiB<sub>2</sub> composite powder, *J. Therm. Anal. Calorim.* vol. 104 (3) (2011) 1063–1070.
- [19] F.S. Alvar, M. Heydari, A. Kazemzadeh, M. Vaezi, L. Nikzad, Al<sub>2</sub>O<sub>3</sub>-TiB<sub>2</sub> nanocomposite coating deposition on titanium by air plasma spraying, *Mater. Today Proc.* vol. 5 (7) (2018) 15739–15743.
- [20] A. Standard, G99, Standard test method for wear testing with a pin-on-disk apparatus, ASTM Int. West Conshohocken, PA (2006).
- [21] X. Li, U. Olofsson, E. Bergseth, Pin-on-disc study of tribological performance of standard and sintered gear materials treated with triboconditioning process: pretreatment by pressure-induced tribofilm formation, *Tribol. Trans.* vol. 60 (1) (2017) 47–57.
- [22] E.M. Sharifi, F. Karimzadeh, M.H. Enayati, Synthesis of titanium diboride reinforced alumina matrix nanocomposite by mechanochemical reaction of Al-TiO<sub>2</sub>-B<sub>2</sub>O<sub>3</sub>, *J. Alloy. Compd.* vol. 502 (2) (2010) 508–512.
- [23] I.E. Gonenli and A.C. Tas, Synthesis of aluminum borate whiskers for metal matrix composites, in III. Ceramic Congress, Proceedings Book, 1996, vol. 2, pp. 85–91.
- [24] H. Li, Z. Li, L. Qi, H. Oy, Effect of extrusion on the thermal expansion behavior of Al<sub>18</sub>B<sub>4</sub>O<sub>33</sub> whisker-Mg composites, *Scr. Mater.* vol. 61 (5) (2009) 512–515.
- [25] X. Tao, X. Wang, X. Li, Nanomechanical characterization of one-step combustion-synthesized Al<sub>14</sub>B<sub>2</sub>O<sub>9</sub> and Al<sub>18</sub>B<sub>4</sub>O<sub>33</sub> nanowires, *Nano Lett.* vol. 7 (10) (2007) 3172–3176.
- [26] A. Alizadeh, M. Geraei, M.R. Mahoodi, In situ fabrication of Al-Al<sub>2</sub>O<sub>3</sub>-TiB<sub>2</sub> hybrid nanocomposite; Evaluating the effect of TiO<sub>2</sub> and B<sub>2</sub>O<sub>3</sub> mechanical milling time on properties of composite created through vortex casting, *Mater. Res. Express* vol. 6 (4) (2019) 45037.
- [27] M.A. Khaghani-Dehaghani, R. Ebrahimi-Kahrizangi, N. Setoudeh, B. Nasiri-Tabrizi, Mechanochemical synthesis of Al<sub>2</sub>O<sub>3</sub>-TiB<sub>2</sub> nanocomposite powder from Al-TiO<sub>2</sub>-H<sub>3</sub>BO<sub>3</sub> mixture, *Int. J. Refract. Met. Hard Mater.* vol. 29 (2) (2011) 244–249.
- [28] B.J. Gill, R.C. Tucker, Plasma spray coating processes, *Mater. Sci. Technol.* vol. 2 (3) (1986) 207–213.
- [29] L. Nikzad, T. Ebadzadeh, M.R. Vaezi, A. Tayebifard, Effect of milling on the combustion synthesis of ternary system B<sub>2</sub>O<sub>3</sub>, Mg and C, *Micro Nano Lett.* vol. 7 (4) (2012) 366–369.
- [30] R. Chaim, M. Hefetz, Effect of grain size on elastic modulus and hardness of nanocrystalline ZrO<sub>2</sub>-3 wt% Y<sub>2</sub>O<sub>3</sub> ceramic, *J. Mater. Sci.* vol. 39 (2004) 3057–3061.
- [31] E. Irom, M. Zakeri, A.S.A. Hossein, Zadeh, "Effect of annealing process on IR transmission and mechanical properties of spark plasma sintered Ytria, *Ceram. Int.* vol. 44 (2) (2018).
- [32] S.N. Alam, L. Kumar, Mechanical properties of aluminium based metal matrix composites reinforced with graphite nanoplatelets, *Mater. Sci. Eng. A* vol. 667 (2016) 16–32.
- [33] P. Gudlur, A. Forness, J. Lentz, M. Radovic, A. Muliana, Thermal and mechanical properties of Al/Al<sub>2</sub>O<sub>3</sub> composites at elevated temperatures, *Mater. Sci. Eng. A* vol. 531 (2012) 18–27.
- [34] A. Leyland, A. Matthews, On the significance of the H/E ratio in wear control: a nanocomposite coating approach to optimised tribological behaviour, *Wear* vol. 246 (1–2) (2000) 1–11.
- [35] A. Khorsand, H. Majidian, M. Farvizi, Wear behavior and microstructure of alumina-mullite-zirconia composites prepared by a novel method: Coating of zircon powder by aluminum alkoxide, *Ceram. Int.* vol. 48 (22) (2022) 33594–33603.
- [36] M. Farvizi, M. Ghanbariha, A. Faraji, Microstructural Characterization and Wear Performance of NiTi-ZrO<sub>2</sub> Composites, *Met. Mater. Int.* vol. 27 (12) (2021) 5407–5424.
- [37] B. Basu, M. Kalin, *Tribology of Ceramics and Composites: A Materials Science Perspective*, John Wiley & Sons, 2011.